

Multispectral and Circular Polarization-Sensitive Carbon Dot-Polydiacetylene Capacitive Photodetector

Nitzan Shauloff, Rajesh Bisht, Yury Turkulets, Rajendran Manikandan, Ahiud Morag, Avi Lehrer, Joshua H. Baraban, Ilan Shalish, and Raz Jelinek*

Multispectral photodetectors (MSPs) and circularly polarized light (CPL) sensors are important in opto-electronics, photonics, and imaging. A capacitive photodetector consisting of an interdigitated electrode coated with carbon dot/anthraquinone-polydiacetylene is constructed. Photoexcitation of the carbon dots induces transient electron transfer to the anthraquinone moieties, and concomitant change in the film dielectric constant and recorded capacitance. This unique photodetection mechanism furnishes wavelength selectivity that is solely determined by the absorbance of the carbon dots incorporated in the anthraquinone-polydiacetylene matrix. Accordingly, employing an array of polymerized-anthraquinone photodetector films comprising carbon dots (C-dots) exhibiting different excitation wavelengths yielded optical “capacitive fingerprints” in a broad spectral range (350–650 nm). Furthermore, circular light polarization selectivity is achieved through chiral polymerization of the polydiacetylene framework. The carbon dot/anthraquinone-polydiacetylene capacitive photodetector features rapid photo-response, high fidelity, and recyclability as the redox reactions of anthraquinone are fully reversible. The carbon dot/anthraquinone-polydiacetylene platform is inexpensive, easy to fabricate, and consists of environmentally friendly materials.

1. Introduction

Multispectral photodetectors are widely used in optical communications,^[1,2] security systems,^[3,4] imaging,^[5,6] household electronics,^[7] molecular identification,^[8] and other applications.^[9–11] Traditional MSPs are based on semiconductor materials grown by epitaxial techniques which are generally not compatible with low-cost large-scale processing.^[12] Additionally, the performance and applicability of MSPs in desired spectral ranges mostly depend on the selection and physical tuning of the band-gap materials employed, considered a challenging task. Moreover, the intrinsic properties of inorganic material MSPs pose significant challenges in modern applications, as they exhibit limited biocompatibility, inadequate mechanical flexibility, and relatively high weight.^[13,14]

MSPs based on organic materials, also referred to as organic photodetectors (OPDs), may provide promising technological avenues. Recent studies reported on-par or better performance of OPDs compared to their inorganic counterparts, in term of wavelength specificity, sensitivity, and size/weight.^[15] Organic MSPs employing photoactive polymers,^[16] small semiconductor organic compounds,^[17] cholesteric liquid crystals,^[18] or nanocomposite carbon-based materials^[19,20] have been reported. While OPDs exhibit in many instances good wavelength tunability, cost effective manufacturing, and simple fabrication processes, their wider practical adoption has been limited due to their oft-encounter disordered structures, low carrier mobilities, and high exciton binding energies.^[13] Capacitive photodetectors constitute an interesting class of OPDs. Capacitive photodetectors based on semiconductor-polymer composites^[21] and single-walled carbon nanotube (SWCNT) layers^[22] have displayed efficient photon absorption and low power consumption. Conceptual and technical challenges for applicability of capacitive photodetector technologies have been encountered, however, including slow response and recovery times, low sensitivity, and complex fabrication processes that are incompatible with large scale fabrication.


Carbon dots, unique carbonaceous nanoparticles, have emerged as useful and versatile nanomaterials in opto-electronic applications due to their tunable optical and electronic

N. Shauloff, R. Bisht, R. Manikandan, A. Morag, A. Lehrer, J. H. Baraban, R. Jelinek

Department of Chemistry
Ben Gurion University of the Negev
Beer Sheva 8410501, Israel
E-mail: razj@bgu.ac.il

Y. Turkulets, I. Shalish
School of Electrical Engineering
Ben Gurion University of the Negev
Beer Sheva 8410501, Israel

R. Jelinek
Ilse Katz Institute for Nanotechnology
Ben Gurion University of the Negev
Beer Sheva 8410501, Israel

 The ORCID identification number(s) for the author(s) of this article can be found under <https://doi.org/10.1002/smll.202206519>.

© 2022 The Authors. Small published by Wiley-VCH GmbH. This is an open access article under the terms of the Creative Commons Attribution-NonCommercial License, which permits use, distribution and reproduction in any medium, provided the original work is properly cited and is not used for commercial purposes.

DOI: 10.1002/smll.202206519

properties.^[23–25] C-dots' photoluminescence can be modulated primarily through surface modification of the nanoparticles.^[26,27] Importantly, C-dots are inexpensive and easy to produce, they are biocompatible and non-toxic, and can be integrated within varied composite materials and matrixes.^[28–30] C-dots have been used as photosensitive components in photodetector designs. Sarkar et al., for example, constructed broadband photodetectors comprising C-dots, reduced Graphene Oxide (rGO), and silver nanoparticles (Ag NPs) on p-doped silicon. In particular, incorporation of C-dots within the rGO/Ag NP layers minimized the dark current and improved the PD responsivity.^[31] In yet another report, C-dots incorporated within a UV photodetector facilitated detection of light at very short wavelengths (down to 254 nm).^[32] C-dot-based photodetectors, however, have had limited applicability mostly due to cumbersome synthesis protocols, complex device fabrication processes, and often slow response/recovery times.^[33–35]

Here we present the construction of a capacitance-based multispectral photodetector, comprising C-dots and anthraquinone-displaying conjugated polydiacetylene (PDA) as the photo-responsive elements. PDA is a unique chromatic polymer, exhibiting visible color properties and used in varied optical sensing applications.^[36] PDA systems have been also employed as a core component in the dielectric medium of capacitive sensors.^[37] Anthraquinone moieties have been widely employed in electrochemical applications, particularly via their participation in reversible redox reactions.^[38,39] We recently showed that polymerized monosubstituted anthraquinone-PDA manifests distinct aggregation-dependent chromatic properties, affected by the alignment of both the aminoanthraquinone headgroups and diacetylene sidechains.^[40]

The anthraquinone-PDA-C-dot capacitive multispectral photodetector presented here features remarkable sensitivity and wavelength selectivity over a broad spectral range (350–650 nm). Importantly, we demonstrate that the wavelength selectivity of the photodetector was directly determined by the light absorbance profile of the C-dots employed, underscoring an intrinsic tunability of the photodetector system. Additionally, the anthraquinone-PDA-C-dot capacitive photodetector can distinguish circularly polarized light through enantioselective polymerization of the Bis-ADA monomer. The anthraquinone-PDA-C-dot capacitive photosensor is readily constructed from inexpensive and environmentally benign materials, and is amenable for large scale production, opening new avenues in organic multispectral photodetector technologies.

2. Results and Discussion

2.1. Design of the Anthraquinone-Polydiacetylene/Carbon Dot Photodetector

Figure 1 illustrates the synthesis scheme of the wavelength- and polarization-sensitive capacitance-based photodetector, employing a mixture of C-dots and polydiacetylene-anthraquinone derivative. The simple synthesis procedure for preparation of bis-anthraquinone-diacetylene (Bis-ADA), the monomeric building block, consisted of amide coupling of 1,5-diaminoanthraquinone and acyl chloride of 10,12-tricosadiynoic acid (**Figure 1A**).

Importantly, π - π stacking interactions between the anthraquinones in Bis-ADA and hydrogen bonding involving the amide residues facilitated formation of the rigid polymerized diacetylene (PDA) network. In particular, the delocalized electrons at the carbonyl units/aromatic unit of anthraquinone, coupled to the conjugated PDA network, are expected to endow Bis-PDA with distinct photophysical properties, utilized in the new photodetector system. **Figure S1**, Supporting Information exhibits the NMR spectrum of Bis-ADA monomer.

Figure 1B portrays construction of the multispectral capacitive photodetector comprising C-dots and polymerized Bis-ADA. Specifically, C-dots and Bis-ADA were drop-casted on the surface of a commercially available interdigitated electrode (IDE) followed by ultraviolet (UV) irradiation to cross link the adjacent diacetylene monomeric units. The resultant polymerized-Bis-ADA/C-dot photodetector produces distinct light-induced capacitive signals that are sensitive to wavelength and circular polarization of the illuminating beam.

The optical and structural properties of the polymerized-Bis-ADA/C-dot films are depicted in **Figure 2**. C-dots were synthesized from ortho-phenylenediamine (oPD) as the carbonaceous precursor (**Figure 2A**). Importantly, hydrothermal treatment of oPD interspersed with different acids in ethanol yielded C-dots exhibiting distinct colors (i.e., distinct fluorescence emissions; photographs showing the C-dot colors upon illumination at 365 nm are presented in **Figure 2A**).^[41] The normalized fluorescence excitation spectra in **Figure 2A,ii** underscore the specific wavelengths, in a broad spectral range, absorbed by the C-dots. Specifically, maximal fluorescence excitations at 400, 440, and 580 nm for blue C-dots, green C-dots, and red C-dots, respectively, were attained (**Figure 2A,ii**). The pertinent excitation-dependent emission spectra of the synthesized C-dots are presented in **Figure S2**, Supporting Information.

Figure 2B illustrates the fabrication process of the polymerized-Bis-ADA/C-dot photodetector film and its morphology. The C-dots were initially interspersed with the Bis-ADA monomers in toluene and drop-casted on the IDE surface. The initial yellowish appearance of the film arises from the anthraquinone moieties within the Bis-ADA monomers. Subsequent UV irradiation (365 nm) generated a green-brownish appearance, corresponding to a color mixture between the blue polymerized PDA and yellow anthraquinone (absorbance spectra of the film recorded at the different assembly stages are provided in **Figure S3**, Supporting Information). The scanning electron microscopy (SEM) image in **Figure 2B** (inset) reveals a typical sheet-like morphology of the aligned polydiacetylene networks.^[42]

Interestingly, the polymerized-Bis-ADA/C-dot film exhibits reversible thermochromism (**Figure 2B**, bottom). Specifically, upon increasing the temperature to 60 °C, the film transformed into a reddish color (**Figure 2B**, bottom left), reflecting the blue-red phase transition of the PDA network.^[43] The polymerized-Bis-ADA/C-dot film reverted to its original green-brownish color at 25 °C (**Figure 2B**, bottom). Reversible thermochromism in PDA systems is closely dependent upon the packing geometries of the polymer pendant sidechains.^[43] As such, the thermochromic reversibility observed in the polymerized-Bis-ADA/C-dot film likely arises from disruption of π - π interactions between the anthraquinone

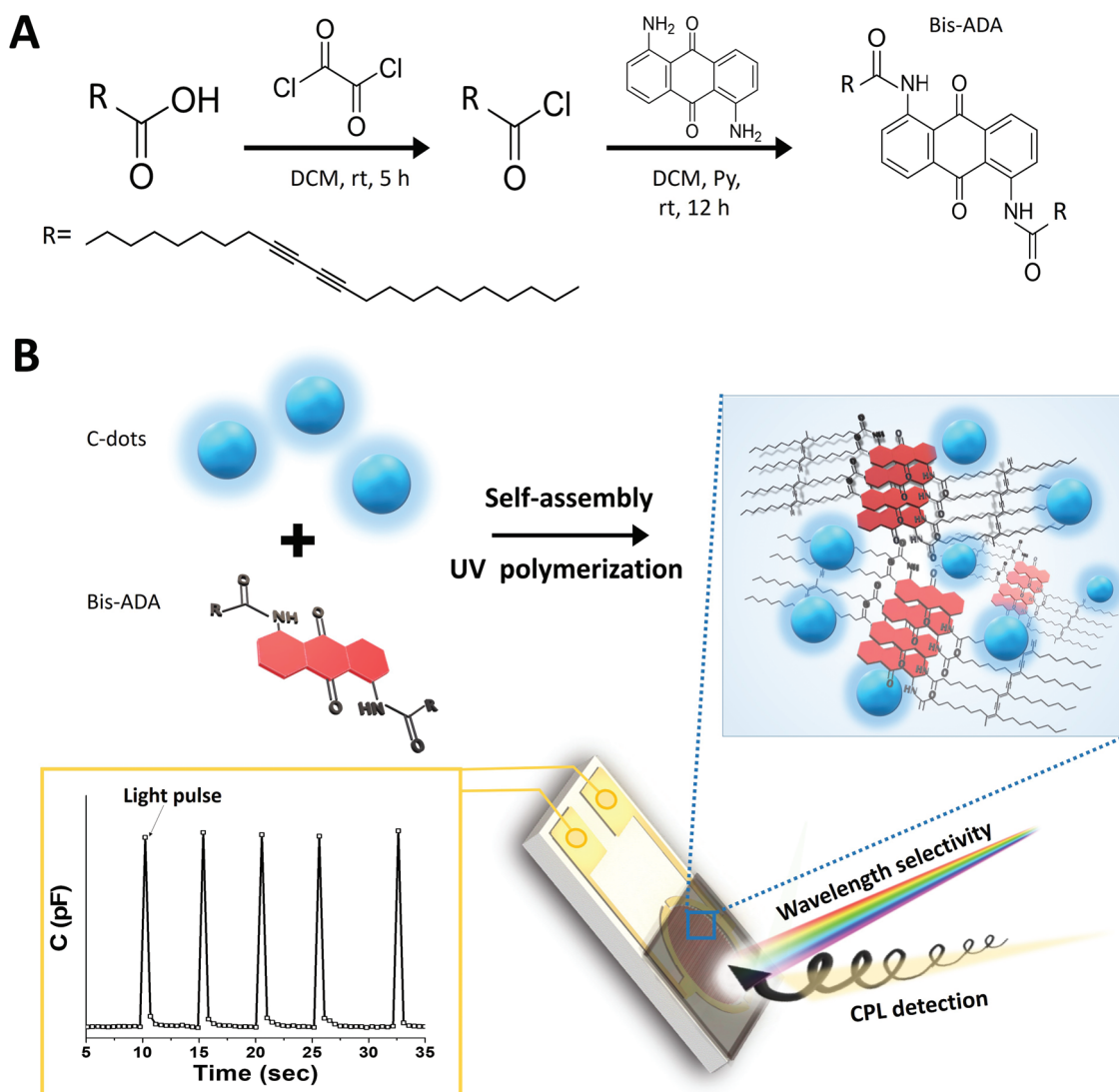


Figure 1. Design of the anthraquinone-polydiacetylene/carbon dot film and photodetector architecture. A) synthesis route of bis-anthraquinone-diacetylene (Bis-ADA) using the 10,12-tricosadiynoic acid precursor. B) Formation of the polymerized-bis-anthraquinone-diacetylene (polymerized-Bis-ADA)/C-dot film on the surface of the interdigitated electrode (IDE); wavelength-dependent and polarization-dependent capacitive signals are induced by illumination.

residues at high temperature and their reconstruction upon lowering the temperature, allowing reversible reorganization of the conjugated PDA network.^[44] Importantly, the colorimetric properties of the polymerized-Bis-ADA/C-dot film highlighted in Figure 2B indicate that the embedded C-dots did not disrupt the assembly and polymerization of the diacetylene monomers.

2.2. Capacitive Photodetection Properties

Figure 3 depicts the capacitance changes induced upon illuminating the polymerized-Bis-ADA/C-dot photodetector, using light generated by a solar simulator (wavelength range of 300–2000 nm; illumination intensity 70 mW cm⁻²). Figure 3A shows the capacitance recorded (presented as percentage

changes) upon exposure to light pulses (500 μs square waves, 70 mW cm⁻² peak-to-peak intensities). Specifically, capacitive transformations which traced the light pulses were recorded in the case of IDE coated with polymerized-Bis-ADA/C-dot films. In contrast, negligible capacitance changes were observed upon application of light pulses using control electrodes that were coated with just C-dots, or only with polymerized-Bis-ADA (Figure 3A). Accordingly, the data in Figure 3A confirm that the capacitive photo response occurred only in the presence of both C-dots and Bis-ADA polymer.

Figure 3B highlights the sensitivity and temporal resolution of the photo-induced capacitance signals. In the experiment, we exposed the polymerized-Bis-ADA/C-dot photodetector to a light pulse having 250 ms duration (70 mW cm⁻², generated by a solar simulator) and recorded the capacitive response. Notably, the ≈40 ms rise time and ≈350 ms fall time are shorter

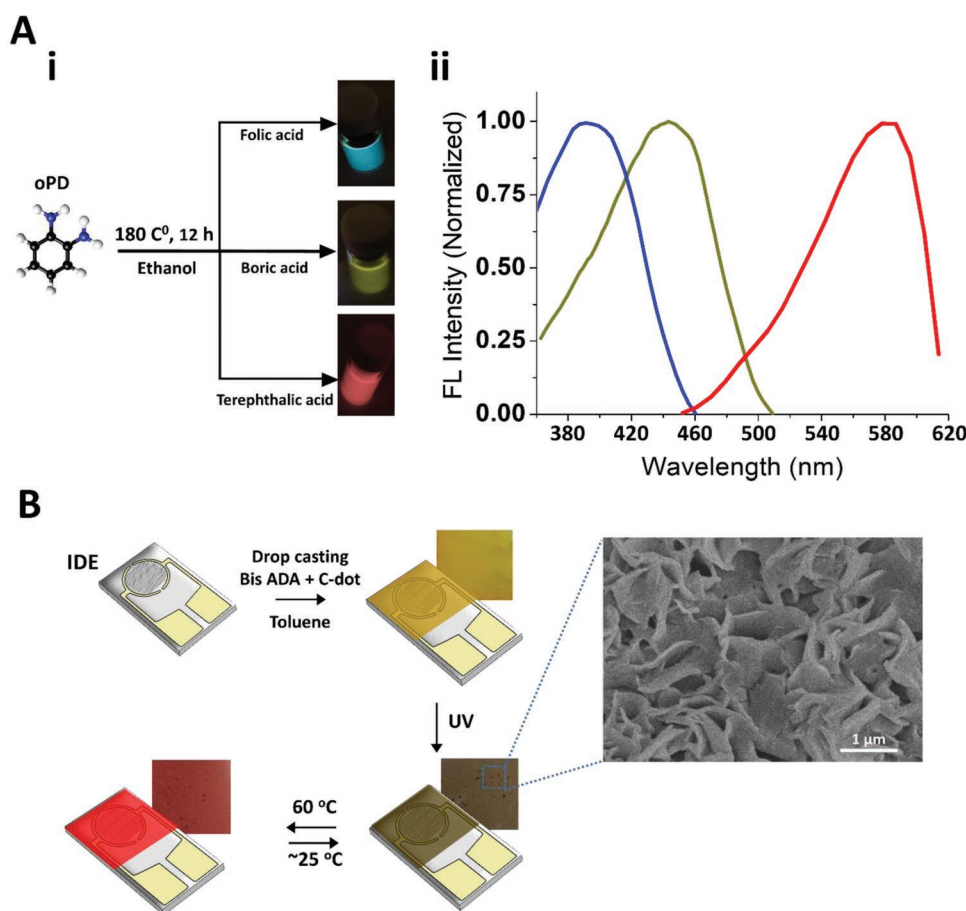


Figure 2. Spectroscopic and microscopic characterization of Bis-anthraquinone diacetylene/carbon-dot films. A) Characterization of the C-dots: i) synthesis of blue C-dots, green C-dots, and red C-dots through hydrothermal treatment of ortho-phenylenediamine in ethanol/acid mixtures. ii) Normalized fluorescence spectra of the three C-dots produced. B) Fabrication of the capacitive photodetector by drop-casting the Bis-ADA monomer and C-dots upon the interdigitated electrode (IDE). Photographs of the generated films are shown in each step. A representative SEM image of the polymerized-Bis-ADA/C-dot film is presented.

than previously published capacitive photodetectors.^[21,45,46] Furthermore, the $\approx 150\%$ capacitance change is large, demonstrating pronounced sensitivity, and dynamic range.

The sensitivity and stability of the photo-induced capacitive signals are further underlined in Figure 3C. The graph in Figure 3C tracks the relative capacitance change ($\Delta C/C_0$) recorded upon continuously illuminating the polymerized-Bis-ADA/C-dot photodetector using different light intensities (illumination intensities in mW cm^{-2} using a white-emitting LED are indicated). Importantly, Figure 3C reveals stability of the photo response in varied light intensities, reflected in the relative plateaus in the time-dependent capacitive signals. In addition, experimentally significant response was apparent even upon illuminating the sensor in low, 5 mW cm^{-2} light beam power, (on par or better than other reported organic photodetectors). The pulse cycle analysis in Figure 3D further underscores the excellent stability and reproducibility of the polymerized-Bis-ADA/C-dot photodetector. Indeed, $<5\%$ capacitive signal variation is apparent even after application of more than 1000 on/off light pulses (250 ms light pulse duration). Excellent temperature stability (up to $100 \text{ }^\circ\text{C}$) was additionally recorded (Figure S4, Supporting Information).

As Figure 3A underlies the role of the C-dots as a core determinant in the light induced capacitive response of the polymerized-Bis-ADA/C-dot photodetector, we further investigated the photo-response of sensor films comprising C-dots exhibiting absorbance at different wavelengths (Figure 4). Figure 4A depicts the capacitance changes recorded upon illuminating three polymerized-Bis-ADA/C-dot photodetectors, each comprising C-dots exhibiting a different light absorbance/emission profile (i.e., blue C-dots, green C-dots, or red C-dots, e.g., Figure 2A). Importantly, we specifically recorded the capacitive response upon illumination at different light wavelengths (generated by single-color cold-mounted LEDs).

The capacitive transformations depicted in Figure 4A demonstrate wavelength dependence, directly linked to the absorbance wavelengths of the C-dots embedded in the polymerized-Bis-ADA matrix. For example, illumination with a 400 nm light gave rise to a maximal capacitance response—of around 50%—in the case of the blue polymerized-Bis-ADA/C-dot photodetector (Figure 4A,i, blue signals). This electrode, in comparison, produced lower capacitive signals ($\approx 25\%$) when illuminated by the LED exhibiting a wavelength of 500 nm (Figure 4A,ii), and even lower still ($<10\%$) in the case of 600 nm light pulses

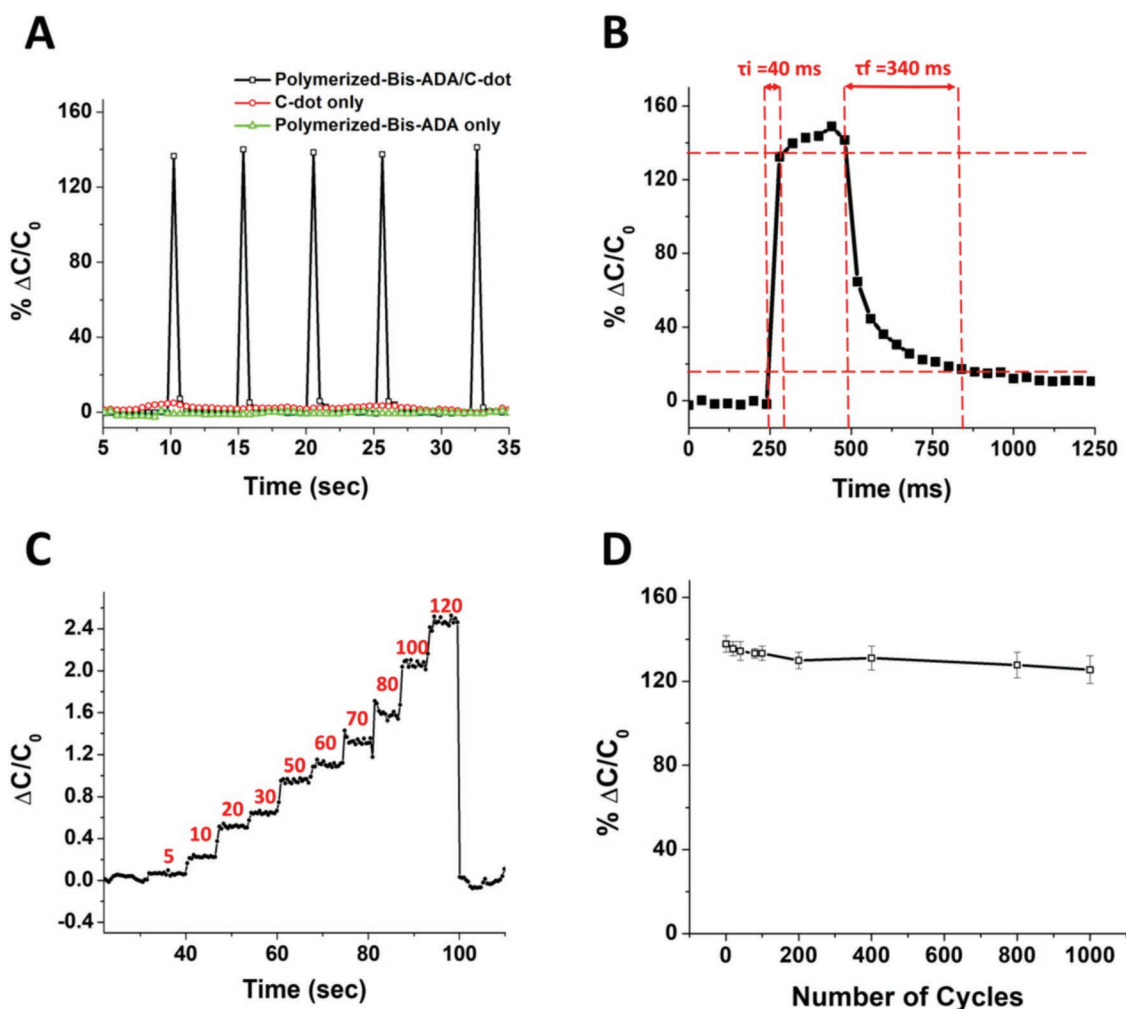


Figure 3. Capacitive photo-response of the polymerized-Bis-anthraquinone-diacetylene/carbon-dot photodetector. A) Capacitance percentage change upon illumination of the polymerized-Bis-ADA/C-dot film-coated IDE with light pulses (generated by a solar simulator at 70 mW cm^{-2} , datapoints collected every 0.3 s). Photoinduced capacitance increase apparent only in the case of polymerized-Bis-ADA film. B) Temporal analysis of the light-induced capacitive signal recorded by polymerized-Bis-ADA/C-dot photodetector upon application of a light pulse (datapoints collected every 0.03 s). C) Light intensity dependence of the photoinduced capacitive signals; the power values of the illuminating light beam (in mW cm^{-2}) are indicated. D) Stability of the photoinduced capacitive signals after repeated application light pulses (250 ms on; 2000 ms off, generated by a solar simulator).

(Figure 4A,iii). Similarly, the most pronounced capacitance change upon illumination at 500 nm was recorded for the green polymerized-Bis-ADA/C-dot photodetector (Figure 4A,ii), while the polymerized-Bis-ADA/red C-dot photodetector produced the highest capacitive signal upon illumination at 600 nm (Figure 4A,iii). The graph in Figure 4B illustrates the overall wavelength dependence of the capacitive response, underlining the key role of the C-dot absorbance wavelength in determining the sensor response.

The capacitive response data obtained upon illumination of the three electrodes (each coated with polymerized-Bis-ADA/C-dot film comprising a different C-dot species) with various monochromatic pulses were classified according to principal component analysis (PCA) (Figure 4C). The PCA graph in Figure 4C underscores the extraordinary capacity of the polymerized-Bis-ADA/C-dot photodetector to distinguish among wavelengths of illuminating light. Specifically, Figure 4C depicts the score plot in the first two principal component

space in which PC1 accounts for the greatest total variation (84.31%), and each point represents three independent capacitive measurements. Importantly, clustering of the experimental datapoints in the PCA plot shows almost no overlaps between the wavelengths tested. Indeed, even though C-dots exhibit in general broad absorbance spectra (e.g., Figure 2A), the use of an electrode array (utilizing different C-dots, as presented in Figure 4C) allows clear distinguishing among wavelengths differing by 50 nm). The photo-induced capacitive “fingerprints” depicted in Figure 4C, obtained with just three electrodes, underscore the power of the photodetector to distinguish wavelengths of incident light; increasing the number of the photodetector array elements (i.e., preparing electrodes deposited with C-dots having different light absorbance profiles) would further enhance the wavelength discrimination capabilities.

Figure 5 demonstrates that the polymerized-Bis-ADA/C-dot photodetector is also capable to distinguish between different

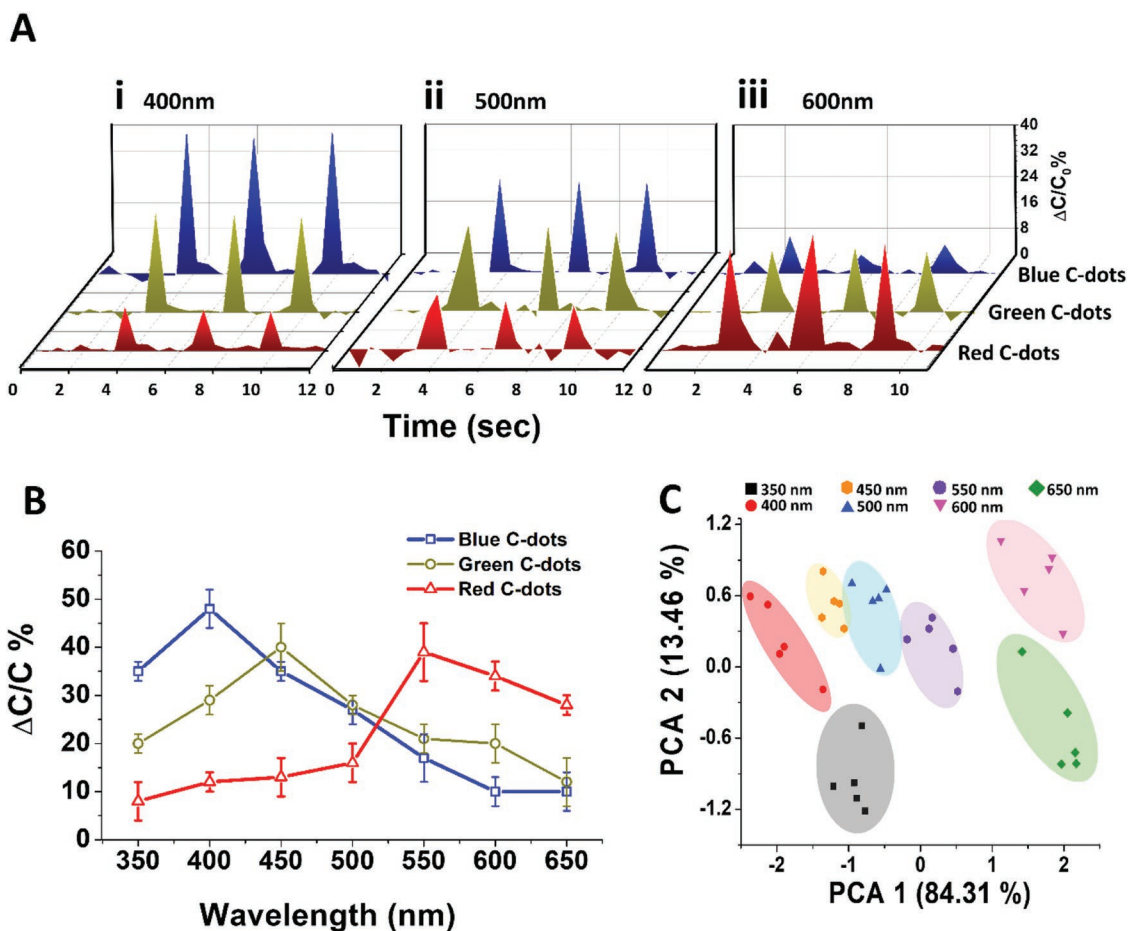


Figure 4. Wavelength selectivity of the polymerized-Bis anthraquinone-diacetylene/carbon dots. A) Photoinduced capacitive response upon light illumination at different wavelengths [i) 400 nm; ii) 500 nm; iii) 600 nm] of polymerized-Bis-ADA/C-dot films comprising blue C-dot (blue), green C-dot (green), or red C-dots (red). B) Capacitance signal intensities recorded in polymerized-Bis-ADA/C-dot films comprising blue C-dot (blue), green C-dot (green) or red C-dots (red), upon illumination at different wavelengths. C) Principal components analysis (PCA) showing capacitive response cluster differentiation according to wavelength illumination.

light circular polarizations (i.e., differentiate light chirality). Deciphering light chirality (left- or right-handed circularly polarized light) is important in varied photonic applications.^[47] In the experiments depicted in Figure 5 we prepared two polymerized-Bis-ADA/C-dot photodetectors, each comprising a different Bis-ADA enantiomer (Left-handed-Bis-ADA and R-handed Bis-ADA, respectively). An enantio-selective polymerization reaction was then carried out through irradiation with circularly polarized visible light (CPVL, generated by 532 nm Nd:YAG laser), using the apparatus shown schematically in Figure 5A.^[48]

The interaction between the CPVL and the Bis-ADA film effectively imposed chiral order in the chain-propagating process. Figure 5B confirms that the two polymerized-Bis-ADA/C-dot films exhibited opposite chirality. Essentially, the circular dichroism (CD) spectra in Figure 5B display positive and negative Cotton effects,^[49] respectively, appearing at 560 and 615 nm with a crossover at 580 nm (blue and red spectra, respectively). The distinctive CD signals are ascribed to chiral polydiacetylene.^[48] Importantly, not inducing chirality of polymerized-Bis-ADA/C-dot films (using non-polarized light at 254 nm for

polymerization) did not give rise to CD signals (Figure 5B, black spectrum).

Sensitivity of the chiral polymerized-Bis-ADA/C-dot photodetector to light polarization is demonstrated in Figure 5C. Specifically, the bar diagram in Figure 5C shows the capacitive responses of left-polymerized-Bis-ADA/C-dot photodetector and right-polymerized-Bis-ADA/C-dot photodetector, respectively, upon illumination with different circularly polarized light (illumination wavelength was 550 nm; C-dots incorporated in the films were red C-dots exhibiting maximal absorbance at 580 nm, e.g., Figure 2B). Indeed, the capacitance response recorded in the experiments reveals matching between light polarization and sensor film chirality. For example, when the left-polymerized-Bis-ADA/C-dot photodetector was illuminated with left-handed CPVL, a pronounced capacitive response of 60% was recorded, while the right handed-CPVL gave rise to lower capacitive signal ($\approx 10\%$, Figure 5C,i). The opposite response to light polarization was observed in the case of right-polymerized-Bis-ADA/C-dot film (Figure 5C,ii). Similar light polarization selectivity was also apparent upon illumination in different wavelengths (i.e., 625 nm, Figure S5, Supporting Information).

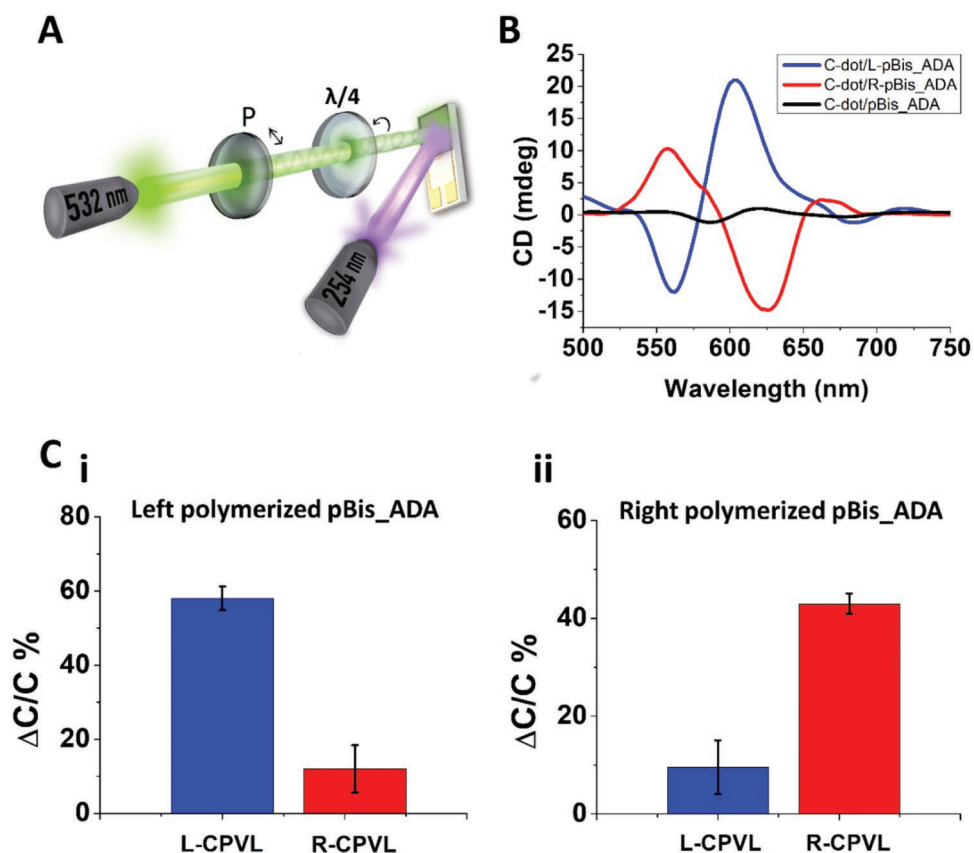


Figure 5. Chiral polymerized-Bis-antraquinone-diacetylene/carbon-dot photodetector distinguishes circularly polarized light. A) Schematic illustration of the enantio-selective polymerization of Bis-ADA afforded by circularly polarized 532 nm Nd:YAG laser, applied simultaneously with non-polarized UV light (16 W UV lamp, $\lambda = 254$ nm). B) Circular dichroism (CD) spectra of red polymerized-Bis-ADA/C-dot film after irradiation with left-handed circularly polarized visible light (CPVL) together with nonpolarized UV light (blue spectrum); right-handed CPVL, and nonpolarized UV light (red spectrum) and nonpolarized UV light alone (black spectrum). C) The measured capacitance response signal under illumination by left-handed-CPVL at 550 nm (blue bars) and right-handed CPVL at 550 nm (red bars) for i) left-polymerized Bis-ADA and ii) right polymerized Bis-ADA, both containing red C-dots.

2.3. Mechanistic Analysis

Figure 6 presents spectroscopic and electrochemical experiments designed to decipher the mechanistic basis of the remarkable capacitive photo-response of the polymerized-Bis-ADA/C-dot system. The normalized fluorescence (NF) spectra in **Figure 6A** (excitation at 254 nm) reflect different radiative transitions of the photo-induced electrons in the films. Notably, the NF peak at around 715 nm, recorded for the polymerized-Bis-ADA/C-dot film (**Figure 6a**, black spectrum), exhibits higher intensity compared to a polymerized-Bis-ADA film alone (**Figure 6a**, green spectrum), indicating that C-dot immobilization gave rise to an increase in the fluorescence intensity of the composite film. In parallel, the major NF signal of the C-dot-only film at around 500 nm (**Figure 6a**, red spectrum) almost completely disappeared in the mixed polymerized-Bis-ADA/C-dot film, likely accounting for non-radiative electron transfer to the polymer. Overall, the NF data in **Figure 6A** indicates that electrons generated in the C-dots through photon absorption are transferred to the embedding polymerized-Bis-ADA matrix through non-radiative processes. Previous studies have shown that C-dots can serve as conduits of light energy transfer to surrounding polymer frameworks.^[50–52]

Surface photovoltage spectroscopy (SPS) analysis of different photodetector film configurations are depicted in **Figure 6B**. SPS monitors changes in the surface voltage as a function of incident photon energy; the technique has been widely employed for optoelectronic characterization of surfaces providing information on charged carrier transitions upon illumination^[53] **Figure 6B** demonstrates differences between the polymerized-Bis-ADA/C-dot film and control samples (C-dots alone, polymerized-Bis-ADA alone). The observed photovoltage recorded in the case of the polymerized-Bis-ADA/C-dot and polymerized-Bis-ADA films indicates photoexcitation and spatial displacement of charged carriers upon illumination. The barely discerned photovoltage in the case of the C-dot-only film attests to the key role of the polymerized-Bis-ADA framework in carrier generation. Importantly, more pronounced (positive) photovoltage was recorded for polymerized-Bis-ADA/C-dot film, likely accounting for the photo-excited electrons transferred from the C-dots to the polymer matrix (e.g., **Figure 6A**) and increasing the abundance of charge carriers.

Figure 6C portrays the proposed mechanism accounting for the photo-induced capacitance changes in the polymerized-Bis-ADA/C-dot system, based upon the photo-induced capacitive response data in **Figures 3–5** and spectroscopic experiments

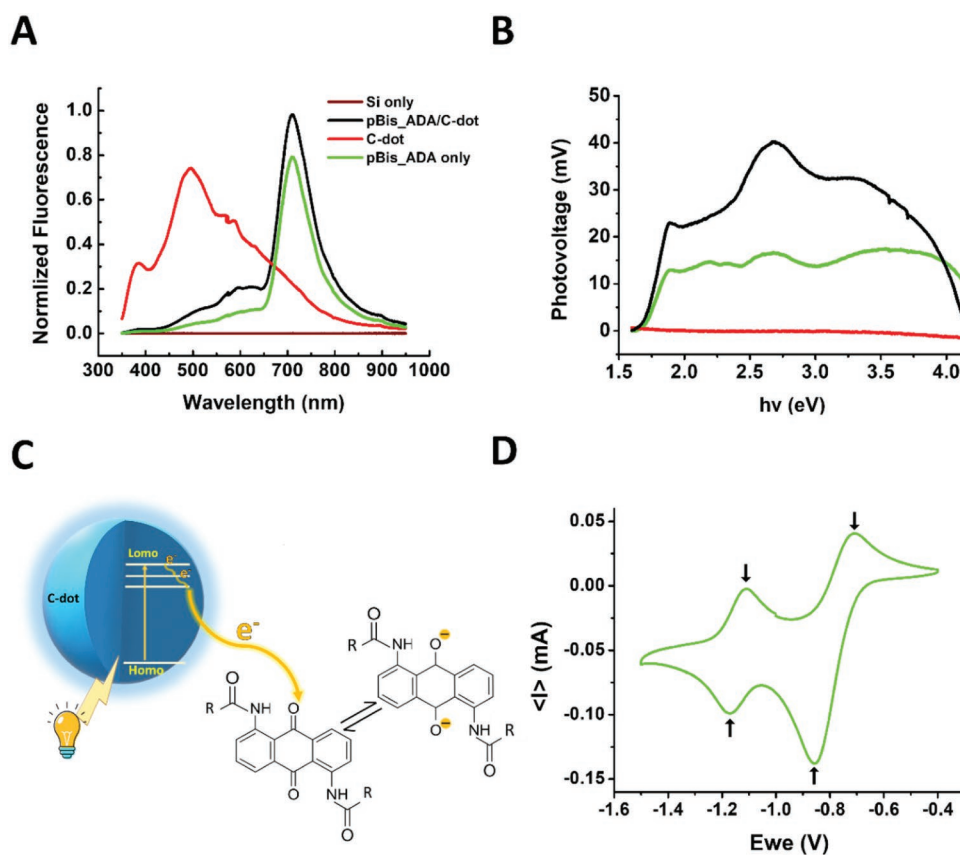


Figure 6. Mechanistic analysis of photo-induced capacitive sensing in the polymerized-Bis-anthraquinone/carbon dot films. A) Normalized fluorescence spectra of the silicon substrate (brown spectrum), deposited C-dots (red spectrum), polymerized-Bis-ADA film (green spectrum), and polymerized-Bis-ADA/C-dot film (black spectrum); excitation was at 254 nm. B) Surface photovoltage spectra (SPS) of films comprising C-dots only (red spectrum), polymerized-Bis-ADA (green spectrum), and polymerized-Bis-ADA/C-dot film (black spectrum). C) Scheme showing the proposed mechanism of light-induced reduction of the quinone moieties in the polymerized-Bis-ADA by photo-excited electrons transferred from proximate C-dots. D) Cyclic voltammetry (CV) curve recorded for polymerized-Bis-ADA/C-dot in 0.1 M tetrabutylammonium-hexafluorophosphate (NBu_4PF_6)/acetonitrile (CAN) deposited on a glassy carbon electrode at a scan rate of 100 mV s^{-1} .

in Figure 6A–B. Specifically, photons absorbed by the C-dots excite electrons between the HOMO and LUMO levels.^[54] The excited electrons consequently migrate to the proximate anthraquinone-polydiacetylene matrix. Similar dissipation of photo-excited electrons from C-dots embedded in polymer matrixes has been previously reported.^[53] Particularly, anthraquinone units have been shown to constitute efficient electron acceptors, undergoing redox transformations.^[55]

Indeed, Figure 6C further highlights a key outcome of electron excitation and consequent electron transfer from the C-dots to the Bis-ADA, specifically the reduction of the anthraquinone residues to anthraquinone-dianions. Indeed, cyclic voltammetry analysis of polymerized-Bis-ADA/C-dot in aprotic solvent mixture (Figure 6D) confirms the occurrence of reduction processes generating the Bis-ADA dianion. In particular, the CV curve in Figure 6D demonstrates that the anthraquinone is electrochemically reduced in a two-step process (indicated by the arrows) usually observed in CV of quinones.^[39] The electric potential values recorded for the reduction peaks (-0.86 and -1.18 V , respectively) and the oxidation peaks (-1.10 and -0.70 V) echo published values, and account for formation of the single anion and subsequent dianion.

The Bis-ADA \rightarrow Bis-ADA²⁻ reduction process due to photo-induced electron transfer from the C-dots likely corresponds to the rapid capacitance changes recorded in the polymerized-Bis-ADA/C-dot system. Specifically, since the dielectric constant (and concomitant capacitance measured) depends upon the polarizability of the molecules in the medium, formation of the doubly charged anthraquinone would result in greater dielectric constants and higher capacitance,^[56] as depicted in the photo-induced capacitive results in Figures 3–5. Indeed, π - π stacking and alignment of the anthraquinone units in the anthraquinone-diacetylene ensemble further affect higher polarizability and enhanced electron mobility contributing to capacitance increase. Indeed, examination of electrodes coated with polymerized diacetylene-anthraquinone consisting of single substituted sidechains (see details in the “Experimental Procedures” section, Supporting Information and the NMR spectra in Figure S4, Supporting Information), or disubstituted diacetylene with anthraquinones on both sides (see details in the “Experimental Procedures” section, Supporting Information and the NMR spectra in Figure S5, Supporting Information), did not exhibit photoinduced capacitance transformations (the capacitance results for these derivatives are shown in Figure S6,

Supporting Information). The two derivatives produced significantly different film morphologies (Figures S7, Supporting Information), particularly not displaying the sheet-like structure of polymerized Bis-ADA which produces the aligned anthraquinone organization and concomitant efficient electron transport.

The mechanistic analysis in Figure 6 also accounts for the distinct sensitivity of the polarized polymerized-Bis-ADA/C-dot to circularly polarized light (e.g., Figure 5). Previous studies have shown that the absorbance and scattering of circularly polarized light interacting with chiral matrixes depend upon surface chirality.^[57,58] In the case of the polymerized-Bis-ADA/C-dot photodetector, the polydiacetylene chirality introduced in the polymerization process^[49] produces a CPVL filtering capacity. Essentially, when the circular polarization of the incident light matches the chirality of polymerized-Bis-ADA, the effective absorbance of light energy accounts for more efficient excitation of the embedded C-dots, giving rise to anthraquinone reduction and more pronounced change of the recorded capacitance, apparent in Figure 5C.

3. Conclusions

We constructed a multispectral organic photodetector comprising an interdigitated electrode coated with a polymerized anthraquinone-diacetylene/C-dot film. The capacitive photo-detection mechanism deciphered relies upon photoinduced excitation of the embedded C-dots, subsequent transient reduction of the quinone residues by the excited electrons, and concomitant modulation of the dielectric constant of the film. The photodetection mechanism enables wavelength selectivity simply through the variation of the type and optical profiles of the embedded C-dots. Indeed, distinguishing among different wavelengths in a broad spectral range was achieved through utilizing an array of C-dot/polymerized-ADA films, in which each film comprised C-dots exhibiting different absorbance wavelengths.

The capacitive polymerized-ADA/C-dot photodetector displays high sensitivity, fast photo-response, reusability, and wavelength selectivity over a broad spectral range. The capacitive photodetection system presented here does not encounter common hurdles in semiconductor-based devices, particularly the requirement of maintaining charge separation in electron-hole pairs which necessitates application of external electrical bias or other methodologies. Similarly, no charge collection is required as the redox reactions responsible for the capacitance transformations are fully reversible. Furthermore, the polymerized-ADA/C-dot IDE films are inexpensive, environmentally benign, easy to synthesize and fabricate, and the technology can be readily upscaled. The polymerized-ADA/C-dot photodetection technology may be implemented in varied applications, including multispectral imaging, full color photodetectors, environmental monitoring, wearable photodetectors, and others.

4. Experimental Section

Materials: Oxalyl chloride (98%, Acros Organic), 1,5-Diaminoanthraquinone (90%, Alfa Aesar), o-phenylenediamine

(oPD), 1-Aminoanthraquinone 97%, folic acid (FA), boric acid 99.5% (BA), terephthalic acid (TPA), Tetrabutylammonium hexafluorophosphate (NBu4PF6, 98%), and *N,N*-Dimethylformamide anhydrous 99.8% (Sigma Aldrich) were used as received. 10,12-tricosadiynoic acid (98%, Alfa Aesar) was purified prior to use by dissolving in chloroform and passing using 0.8 μm syringe filter followed by solvent removal by rotatory evaporation. All organic solvents were purchased from Bio-Lab Ltd., Jerusalem, Israel. Interdigitated gold electrodes (Dimensions: 10 × 6 × 0.75 mm; glass substrate; Insulating layer: EPON SU8 resin; electrode material: Au; electrode thickness: 150 nm; microelectrode with: 10 μm, microelectrode gap: 10 μm; number of fingers: 90 pairs; surface of tested area: 0.86 mm²) were purchased from MicruX Technologies (Oviedo, Spain).

Synthesis of C-Dots: Synthesis of the C-dots was based upon reported procedures for construction of multi-colored C-dots through a scalable acid reagent engineering strategy.^[41] Briefly, in the case of blue C-dots, 500 mg of oPD and 500 mg of FA were dissolved in 10-mL ethanol solution. Subsequently, the solution was transferred into a 25-mL Teflon-lined stainless-steel autoclave and heated at 180 °C for 12 h. After cooling to room temperature, the solution was filtered with a 0.22-μm microporous membrane, and the C-dots were further purified by dialysis in ethanol. C-dot powder was obtained for further characterization after evaporation. Green C-dots and red C-dots were prepared using a procedure similar as described above using different acid mixtures. Specifically, 500 mg of BA or TPA was used to react with oPD (500 mg) for green C-dots and red C-dots, respectively.

Synthesis of Bis-Anthraquinone-Diacetylene (Bis-ADA): See details in the Supporting Information.

Polymerized-Bis-ADA/C-Dot Photodetector: To prepare the polymerized-Bis-ADA/C-dot interdigitated electrodes (IDEs) capacitive electrodes, a recently developed protocol was utilized.^[59] Briefly, 7.5 mg of C-dot were mixed with 15 mg Bis-ADA monomer dissolved in 1 mL of toluene. The solution was then drop-casted (10 μL) on the surface of the IDEs and dried for 2 h at room temperature. The resultant coated electrodes were further irradiated for 2 min with a UV lamp (254 nm, 16 W) to induce PDA cross-linking in ambient atmosphere. The color of the deposited composite film changed from yellowish-green color to dark brown, further transforming to red after annealing on a hot plate (80 °C for 1 min). Five electrodes were employed in each experiment.

Photo-Response Measurements: Capacitive photo-response measurements of the polymerized C-dot-Bis-ADA-IDE devices were carried out using an LCR meter (Keysight Technologies, E4980AL Precision LCR Meter). For the light source, a white light emitting diode (LED, Chanzon, China) operating in a wavelength range of 380–800 nm and a mounted LED sources with wavelength centered at 300-nm (UV), 365-nm (UV), 405-nm (violet), 450-nm (blue), 505-nm (cyan), 554-nm (green), 600-nm (orange), and 645-nm (red) LEDs from Thorlabs (Newton, New Jersey, United States) were used. Light intensity was measured using a power meter (PM100, Thorlabs) while applying the illumination.

Capacitive measurements were performed at room temperature upon exposure of the polymerized C-dot-Bis-ADA-IDE devices to the different light sources. Capacitance values were recorded after reaching a clear baseline, collecting the data every 0.03 and 0.3 s at 1 kHz constant frequency with a voltage of 1 V. Thorlabs DC2200a LED driver was used in the pulsed light experiments.

Data Analysis: The IDE photoinduced capacitance depends on variations of the dielectric constant of the deposited film. Capacitance of the interdigital electrode was defined by the Equation:

$$C = \eta \epsilon_0 \epsilon_r \frac{lt}{d} \quad (1)$$

where C is the capacitance in farads (F), η is the number of fingers (90 in the IDE employed here), ϵ_0 is the permittivity of free space ($\epsilon_0 = 8.854 \times 10^{-12}$ F m⁻¹), ϵ_r is the relative permittivity, also known as the dielectric constant, t is the thickness of interdigital electrodes, l is the length of interdigital electrodes, and d is the distance between the electrodes. The capacitance response of the sensors— ΔC —was defined

as $C_{\text{light}} - C_{\text{dark}}$, where C_{light} and C_{dark} are the capacitance value after illumination and the capacitance baseline value measured under dark conditions, respectively. Capacitance percentage change was calculated to compare between the electrodes.

Enantio-Selective Polymerization of Bis-Anthraquinone-Diacetylene: The enantio-selective polymerization reactions were carried out based on published procedures.^[50] Briefly, circular polarized visible light (CPVL) was created by passing a laser light (532 nm Nd:YAG Semiconductor laser, light intensity 30 mW cm^{-2}) through a linear polarizer plus a $\lambda/4$ waveplate. Chiral Polymerization was applied through simultaneous irradiation with CPVL and non-polarized UV light (16 W UV lamp, $\lambda = 254 \text{ nm}$) at 450 nm in order to form the enantio-selective polymerization. CD spectra were measured by placing the film sample perpendicular to the light path using JASCO CD spectrometer J-810.

Characterization: Scanning electron microscopy (SEM) images of the films on IDE were acquired after air-drying overnight. Dried sample was covered with 5 nm of Au sputtering. The samples were imaged using a FEI Verios, SEM (Thermo Fisher Scientific, XHR 460L). The images were viewed at different magnifications, in an acceleration voltage of 5 kV. UV-vis absorbance spectra were recorded on Thermo Scientific Evolution 220 spectrophotometer in the range of 300–800 nm at room temperature. Fluorescence spectra of C-dot solutions were recorded using a fluorescence spectrophotometer (Horiba, Japan). Fluorescence emissions were measured at different excitation wavelengths ranging from 360 to 620 nm. The fluorescence was measured at a 90° angle relative to the excitation light. This geometry was used instead of placing the sensor at the line of the excitation light at a 180° angle to avoid interference of the transmitted excitation light. Fluorescence spectra of the deposited films on a silicon wafer were acquired on a Newport Corp. MS257 spectrometer equipped with a Si CCD detector and long-pass order-sorting filters. A 1-mW He-Cd laser was used for excitation. Circular dichroism (CD) spectra were recorded in the range of 500–750 nm at room temperature on a Jasco J-715 spectropolarimeter, using an optical path length of 0.1-mm via quartz plate cuvettes. The plate cuvettes were coated with a thin film composed of C-dot/L-polymerized-Bis-ADA, C-dot/R-polymerized-Bis-ADA, and a control of C-dot/polymerized-Bis-ADA. The CD spectra were measured by placing the film perpendicular to the light path. Cyclic voltammetry (CV) measurements were performed in a three-electrode configuration, with polymerized sample on a glassy carbon electrode (GCE) as the working electrode, Pt wire as the counter electrode, and Ag/AgCl as the reference electrode. 0.1 M NBu₄PF₆ in Acetonitrile was used as the aprotic electrolyte, and the measurements were performed at a scan rate of 100 mV s^{-1} at a voltage range of -0.4 to -1.5 V versus Ag/AgCl. The experiments were performed on a BioLogic SP-150 instrument (Seysinet-Pariset, France). Prior to material deposition, the glassy carbon electrode was cleaned by polishing with $0.25 \mu\text{m}$ diamond polishing compound, then rinsing with copious amounts of DI water, followed by a second polish with a $0.05 \mu\text{m}$ alumina slurry and a final rinse with DI water. Surface photovoltage spectra (SPS) were acquired on films deposited on Si templates having a ground contact on their periphery. The photovoltage signal was acquired using a Besocke Delta Phi GmbH Kelvin probe from samples placed in a dark Faraday cage at room temperature. The samples were illuminated using a 300 W Xe light source monochromatized by Newport Corp. MS257 monochromator. To prevent illumination by second order diffractions of the grating, the monochromatized light was further filtered by order-sorting long pass filters. The photon flux was kept constant throughout the entire spectral acquisition by means of a variable slit operated in closed control loop.

Supporting Information

Supporting Information is available from the Wiley Online Library or from the author.

Acknowledgements

The authors are grateful to Prof. Idan Hod for help with the LED setup. R.J. is grateful to the Israel Science Foundation for financial support (Grant no. 1657/20).

Conflict of Interest

The authors declare no conflict of interest.

Data Availability Statement

The data that support the findings of this study are available in the supplementary material of this article.

Keywords

capacitive photodetectors, carbon dots, circularly polarized light detection, multispectral photodetectors, polydiacetylene

Received: October 22, 2022

Published online:

- [1] T. Mueller, F. Xia, P. Avouris, *Nat. Photonics* **2010**, *4*, 297.
- [2] H. Chen, H. Liu, Z. Zhang, K. Hu, X. Fang, H. Y. Chen, H. Liu, Z. M. Zhang, K. Hu, X. S. Fang, *Adv. Mater.* **2015**, *28*, 403.
- [3] S. Yuan, R. Yu, C. Ma, B. Deng, Q. Guo, X. Chen, C. Li, C. Chen, K. Watanabe, T. Taniguchi, F. J. García De Abajo, F. Xia, *ACS Photonics* **2020**, *7*, 1206.
- [4] S. Yang, S. Jiao, Y. Nie, H. Lu, S. Liu, Y. Zhao, S. Gao, D. Wang, J. Wang, Y. Li, *J. Mater. Chem. C Mater.* **2022**, *10*, 8364.
- [5] D. Wu, C. Guo, Z. Wang, X. Ren, Y. Tian, Z. Shi, P. Lin, Y. Tian, Y. Chen, X. Li, *Nanoscale* **2021**, *13*, 13550.
- [6] F. H. L. Koppens, T. Mueller, P. Avouris, A. C. Ferrari, M. S. Vitiello, M. Polini, *Nat. Nanotechnol.* **2014**, *9*, 780.
- [7] D. Zhang, C. Fuentes-Hernandez, R. Vijayan, Y. Zhang, Y. Li, J. W. Park, Y. Wang, Y. Zhao, N. Arora, A. Mirzazadeh, Y. Do, T. Cheng, S. Swaminathan, T. Starner, T. L. Andrew, G. D. Abowd, *npj Flexible Electron.* **2022**, *6*, 7.
- [8] K. W. Bentley, C. Wolf, *J. Org. Chem.* **2014**, *79*, 6517.
- [9] Q. Li, J. van de Groep, Y. Wang, P. G. Kik, M. L. Brongersma, *Nat. Commun.* **2019**, *10*, 4982.
- [10] O. Hayden, R. Agarwal, C. M. Lieber, *Nat. Mater.* **2006**, *5*, 352.
- [11] F. Djéffal, N. Boubiche, H. Ferhati, J. Faerber, F. L. e Normand, N. Javahiraly, T. Fix, *J. Alloys Compd.* **2021**, *876*, 160176.
- [12] J. R. Manders, T. H. Lai, Y. An, W. Xu, J. Lee, D. Y. Kim, G. Bosman, F. So, *Adv. Funct. Mater.* **2014**, *24*, 7205.
- [13] H. Ren, J. De Chen, Y. Q. Li, J. X. Tang, *Adv. Sci.* **2021**, *8*, 2002418.
- [14] X. Xu, X. Zhou, K. Zhou, Y. Xia, W. Ma, O. Inganäs, *Adv. Funct. Mater.* **2018**, *28*, 1805570.
- [15] P. C. Y. Chow, T. Someya, *Adv. Mater.* **2020**, *32*, 1902045.
- [16] Z. Zhong, K. Li, J. Zhang, L. Ying, R. Xie, G. Yu, F. Huang, Y. Cao, *ACS Appl. Mater. Interfaces* **2019**, *11*, 14208.
- [17] J. Vanderspikken, W. Maes, K. Vandewal, *Adv. Funct. Mater.* **2021**, *31*, 2104060.
- [18] A. Y.-G. Fuh, S.-J. Ho, S.-T. Wu, M.-S. Li, *Appl. Opt.* **2014**, *53*, 1658.
- [19] T. F. Zhang, Z. P. Li, J. Z. Wang, W. Y. Kong, G. A. Wu, Y. Z. Zheng, Y. W. Zhao, E. X. Yao, N. X. Zhuang, L. B. Luo, *Sci. Rep.* **2016**, *6*, 38569.

- [20] D. de Fazio, B. Uzlu, I. Torre, C. Monasterio-Balcells, S. Gupta, T. Khodkov, Y. Bi, Z. Wang, M. Otto, M. C. Lemme, S. Goossens, D. Neumaier, F. H. L. Koppens, *ACS Nano* **2020**, *14*, 11897.
- [21] S. Jun, S. bin Choi, C. J. Han, Y. T. Yu, C. R. Lee, B. K. Ju, J. W. Kim, *ACS Appl. Mater. Interfaces* **2019**, *11*, 4416.
- [22] S. Smirnov, I. v. Anoshkin, A. Generalov, D. v. Lioubtchenko, J. Oberhammer, *RSC Adv.* **2019**, *9*, 14677.
- [23] F. Yuan, S. Li, Z. Fan, X. Meng, L. Fan, S. Yang, *Nano Today* **2016**, *11*, 565.
- [24] T. Yuan, T. Meng, P. He, Y. Shi, Y. Li, X. Li, L. Fan, S. Yang, *J. Mater. Chem. C Mater.* **2019**, *7*, 6820.
- [25] T. Feng, S. Tao, D. Yue, Q. Zeng, W. Chen, B. Yang, *Small* **2020**, *16*, 2001295.
- [26] K. Holá, M. Sudolská, S. Kalytchuk, D. Nachtigallová, A. L. Rogach, M. Otyepka, R. Zbořil, *ACS Nano* **2017**, *11*, 12402.
- [27] N. Shauloff, A. Morag, K. Yaniv, S. Singh, R. Malishev, O. Paz-Tal, L. Rokach, R. Jelinek, *Nanomicro Lett.* **2021**, *13*, 112.
- [28] J. Liu, R. Li, B. Yang, *ACS Cent. Sci.* **2020**, *6*, 2179.
- [29] S. Pandiyan, L. Arumugam, S. P. Sreirengan, R. Pitchan, P. Sevugan, K. Kannan, G. Pitchan, T. A. Hegde, V. Gandhirajan, *ACS Omega* **2020**, *5*, 30363.
- [30] N. Shauloff, S. Bhattacharya, R. Jelinek, *Carbon N Y* **2019**, *152*, 363.
- [31] K. Sarkar, P. Devi, A. Lata, R. Ghosh, P. Kumar, *J. Mater. Chem. C Mater.* **2019**, *7*, 13182.
- [32] Q. Zhang, J. Jie, S. Diao, Z. Shao, Q. Zhang, L. Wang, W. Deng, W. Hu, H. Xia, X. Yuan, S. T. Lee, *ACS Nano* **2015**, *9*, 1561.
- [33] A. Subramanian, J. Akram, S. Hussain, J. Chen, K. Qasim, W. Zhang, W. Lei, *ACS Appl. Electron. Mater.* **2020**, *2*, 230.
- [34] D. A. Nguyen, H. M. Oh, N. T. Duong, S. Bang, S. J. Yoon, M. S. Jeong, *ACS Appl. Mater. Interfaces* **2018**, *10*, 10322.
- [35] S. Miao, Y. Cho, *Front. Energy Res.* **2021**, *9*, 666534.
- [36] X. Sun, T. Chen, S. Huang, L. Li, H. Peng, *Chem. Soc. Rev.* **2010**, *39*, 4244.
- [37] V. K. Rao, N. Shauloff, X. M. Sui, H. Daniel Wagner, R. Jelinek, R. Jelinek, *J. Mater. Chem. C Mater.* **2020**, *8*, 6034.
- [38] W. Yin, A. Grimaud, I. Azcarate, C. Yang, J. M. Tarascon, *J. Phys. Chem. C* **2018**, *122*, 6546.
- [39] D. Bao, S. Ramu, A. Contreras, S. Upadhyayula, J. M. Vasquez, G. Beran, V. I. Vullev, *J. Phys. Chem. B* **2010**, *114*, 14467.
- [40] R. Bisht, V. Dhyani, R. Jelinek, *Adv. Opt. Mater.* **2021**, *9*, 2001497.
- [41] L. Wang, W. Li, L. Yin, Y. Liu, H. Guo, J. Lai, Y. Han, G. Li, M. Li, J. Zhang, R. Vajtai, P. M. Ajayan, M. Wu, *Sci. Adv.* **2020**, *6*, eabb6772.
- [42] C. Khanantong, N. Charoenthai, S. Wacharasindhu, M. Sukwattanasinitt, W. Yimkaew, N. Traiphol, R. Traiphol, *Colloids Surf. A Physicochem. Eng. Asp.* **2020**, *603*, 125225.
- [43] J. Nuck, K. Sugihara, *Macromolecules* **2020**, *53*, 6469.
- [44] S. Lee, J. Lee, M. Lee, Y. K. Cho, J. Baek, J. Kim, S. Park, M. H. Kim, R. Chang, J. Yoon, *Adv. Funct. Mater.* **2014**, *24*, 3699.
- [45] Y. Hwang, Y. H. Hwang, K. W. Choi, S. Lee, S. Kim, S. J. Park, B. K. Ju, *Sci. Rep.* **2021**, *11*, 10499.
- [46] A. Gencer Imer, A. Dere, A. G. Al-Sehemi, O. Dayan, Z. Serbetci, A. A. Al-Ghamdi, F. Yakuphanoglu, *Appl. Phys. A Mater. Sci. Process.* **2019**, *125*, 204.
- [47] T. Liu, W. Shi, W. Tang, Z. Liu, B. C. Schroeder, O. Fenwick, M. J. Fuchter, *ACS Nano* **2022**, *16*, 2682.
- [48] G. Yang, L. Han, H. Jiang, G. Zou, Q. Zhang, D. Zhang, P. Wang, H. Ming, *Chem. Commun.* **2014**, *50*, 2338.
- [49] C. He, Z. Feng, S. Shan, M. Wang, X. Chen, G. Zou, *Nat. Commun.* **2020**, *11*, 1188.
- [50] L. Mishra, R. K. Behera, S. Mondal, S. Kumar, A. Panigrahi, M. K. Sarangi, *Carbon N Y* **2021**, *178*, 594.
- [51] D. W. M. Pincher, C. A. Bader, J. D. Hayball, S. E. Plush, M. J. Sweetman, *Chem. Sel.* **2019**, *4*, 9640.
- [52] B. Wang, Y. Yu, H. Zhang, Y. Xuan, G. Chen, W. Ma, J. Li, J. Yu, *Adv. Mater.* **2019**, *131*, 18614.
- [53] L. Kronik, Y. Shapira, *Surf. Sci. Rep.* **1999**, *37*, 1.
- [54] H. Nie, M. Li, Q. Li, S. Liang, Y. Tan, L. Sheng, W. Shi, S. X. A. Zhang, *Chem. Mater.* **2014**, *26*, 3104.
- [55] Q. Chang, Z. Song, C. Xue, N. Li, S. Hu, *Mater. Lett.* **2018**, *218*, 221.
- [56] N. Gamboa-Valero, P. D. Astudillo, M. A. González-Fuentes, M. A. Leyva, M. D. J. Rosales-Hoz, F. J. González, *Electrochim. Acta* **2016**, *188*, 602.
- [57] C. Zhang, S. Li, X. Dong, S. Zang, *Aggregate* **2021**, *2*, e48.
- [58] W. Li, Z. J. Coppens, L. v. Besteiro, W. Wang, A. O. Govorov, J. Valentine, *Nat. Commun.* **2015**, *6*, 8379.
- [59] N. Shauloff, N. L. Teradal, R. Jelinek, *ACS Sens.* **2020**, *5*, 1573.